Accepted Manuscript

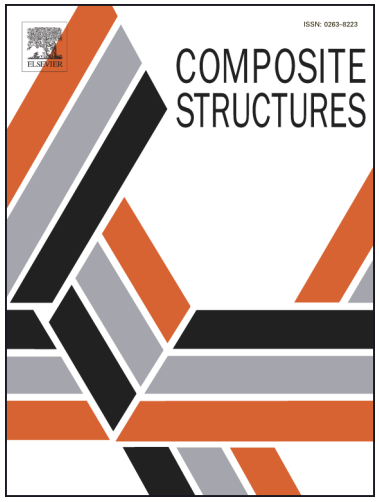

Experimental and numerical analysis of thick embedded laminated glass connections

Manuel Santarsiero, Chiara Bedon, Christian Louter

PII: S0263-8223(17)33679-6
DOI: https://doi.org/10.1016/j.compstruct.2018.01.002
Reference: COST 9242

To appear in: *Composite Structures*

Received Date: 5 November 2017
Revised Date: 18 December 2017
Accepted Date: 2 January 2018

Please cite this article as: Santarsiero, M., Bedon, C., Louter, C., Experimental and numerical analysis of thick embedded laminated glass connections, *Composite Structures* (2018), doi: https://doi.org/10.1016/j.compstruct.2018.01.002

Experimental and numerical analysis of thick embedded laminated glass connections

Manuel Santarsiero[1]*, Chiara Bedon[2], Christian Louter[3]

Abstract

Laminated glass components are usually realized by bonding glass plates using interlayer polymers that develop adhesion forces during lamination. Recently, these adhesion forces have been used also to realize special adhesive connections for structural glass components and assemblies. The typical example of such a joining technique is conventionally known as "embedded laminated connection", where a metal insert is encapsulated in multi-ply laminated glass components.

In this study, careful consideration is paid for the investigation of the mechanical behaviour of embedded laminated connections with thick metal insert. To this aim, small-scale laboratory tests, Finite Element (FE) numerical models and analytical considerations are presented. Firstly, the results of experimental investigations at different temperatures are discussed, giving evidence of the geometrical and mechanical parameter effects on the so observed performances. It is observed, in particular, that the temperature markedly affects not only the maximum load carrying capacity but also the failure mode of the studied connection typology. Non-linear numerical simulations are then developed in ABAQUS on refined FE models, able to account for the geometrical and mechanical properties of the reference connection specimens. Further analytical considerations are also presented, in support of the observed experimental findings. It is shown, in particular, that as far as high temperatures are not attained, the mechanical performance and failure mode of the examined connections is strictly related to glass breakage. In addition it is also observed that at high temperature, failure mode (i.e. bubble formation) and failure location are in line with the expectations. Rather close correlation can be also found for the same embedded connections between test results, FE numerical simulations and analytical assumptions.

Keywords: laminated glass connections, adhesives, thick metal insert, experimental testing, numerical modelling, temperature

[1] Structural and R&D Engineer, Eckersley O'Callaghan, London, United Kingdom. (*) Corresponding Author
[2] Assistant Professor, University of Trieste, Department of Engineering and Architecture, Trieste, Italy
[3] Assistant Professor, Delft University of Technology, Faculty of Architecture and the Built Environment, Department of Architectural Engineering and Technology, Delft, The Netherlands

1. Introduction and state-of-the-art

In the design of structural systems, a multidisciplinary approach and specific *fail-safe* design criteria are generally required to offer appropriate performance levels (i.e. [1, 2]), including advanced analysis methods able to account for the intrinsic properties of glass, as well as loading and boundary conditions. There, the connections between structural glass components represent one of the major issues to assess in the structural design of glass elements and even complex assemblies. The load application and the load transfer between different elements are in fact indeed rather critical, given the fragile nature of glass, as well as the sensitivity of adhesives and interlayers to temperature and loading conditions [1, 2]. The structural interaction between multiple structural components is in fact assigned to connection elements and details composed of specific materials, whose mechanical performance has to be properly assessed.

A common technique to connect glass elements - being largely used since 60s - is represented by bolted connections. However, it is also recognized that such a solution is affected by several disadvantages, like for example the stress intensification at the borehole edges and reduced material resistance due to the drilling process [1, 2]. Recently, adhesive connections have been studied (i.e. [3]-[9]) and used in architectural applications ([10]-[12]) as an effective alternative to mechanical bolted connections. Indeed, adhesive connections do not require drilling of the glass and they transfer load over a larger area, than is typically done in a bolted connection.

The current study focuses on a specific typology of adhesive connections, called “embedded laminated connections”. There, a metal insert is directly laminated inside the laminated glass component, i.e. “embedded”, rather than externally bonded to the glass surface as in use for other adhesive joints. Embedded laminated connections make therefore use of the laminated interlayer to transfer loads from the metal insert to the glass panels. Earlier research efforts, in this regard (see [13]-[16]), have been dedicated to embedded connections with a “thin” metal plate laminated within the interlayer. Compared to existing investigations, a “thick” metal insert is used for connections explored in this paper, i.e. by assuming the same thickness for the metal component and the adjacent glass panel.

Small-scale investigations carried out at the connection level are hence here presented and discussed, including pull-out experimental testing, FE numerical simulations and analytical considerations. The experimental tests and related outcomes are first presented in section 3, where - given the well-known temperature dependent behaviour of the interlayer adhesive - pull-out tests performed at different temperatures are discussed. The full set of experiments included 12 small-scale specimens. In order to further explore the mechanical behaviour of the examined connection technique, test results and experimental observations were then compared to FE numerical simulations (ABAQUS [17]) and analytical studies (see section 4), giving evidence of their overall response and typical failure mechanism. Finally (section 5), a concise FE parameter study is briefly discussed, aiming to

preliminary investigate the effect of some key input parameters on the mechanical response of the same connections.

2. Design concept and materials

The reference small-scale specimen of embedded laminated connections investigated in this study consists in a laminated glass plate (300mm×150mm the nominal dimensions) with an embedded metal insert. The laminated glass panel consists of three plies of annealed glass [18], bonded by means of two 1.5mm thick SentryGlas® (SG) ionomer adhesive interlayer foils [19]. The nominal thicknesses of the glass plies are 6mm and 10mm, for the outer and middle plies respectively. The metal insert, consisting of 316L stainless steel [20], is embedded in the laminated glass pane along one long edge (see also Figures 1 and 2(a)). For clarity of presentation, as also in accordance with Figure 1, the label "frontal edge" is used to detect the long edge of the insert, while the "lateral edge" is the short one. Before assembling the specimens, all the surfaces of the metal insert are polished, to mirror quality (i.e. dimension tolerances h9 and bonded surface machined with roughness of 8μm).. Similarly, silane primer is applied to the embedded surfaces to ensure good adhesion quality with SG foils. Through the full assembly process, special bespoke devices are used, so to (i) ensure the correct position of the metal inserts; (ii) prevent inserts rotation during the lamination and (iii) ensure the alignment of the glass edges (within a tolerance of 0.5mm from the nominal geometry).

In the numerical analysis presented in this work, it is assumed that the stress in glass plates are equal to zero when the specimens is unloaded. From literature, it is known that a limited residual compressive stress (i.e. in the range of -0÷-4MPa) typically occurs in regular (non-laminated) panes of annealed glass. However, it is expected that further residual stresses might be developing in the glass during lamination. Because of this reason, the residual stress profile in the outer glass ply of the laminated annealed glass components was measured after lamination. More in details, surface stress values were measured along x-path (see Figure AII-2) by means of scattered-light-polariscope (SCALP-05, GlasStress Ltd.) [21]. From these measurements, a change in residual stress level between the region far away and the region close to the metal insert was observed. More specifically, a residual compressive stress level of about -0÷-3MPa was measured far away from the metal insert, whereas a disturbance in the residual stress level was measured more close to the metal insert and a residual tensile stress up to +6MPa was measured at the metal insert. These findings indicate that laminating an embedded metal insert in a laminated glass component does have a measurable effect on the residual stress distribution in the glass. This effect could derive from the different thermal expansion of metal and glass elements. A similar consideration is in fact also in line with the experimental observation. Although such a magnitude of residual stress is not expected to have a significant effect on the results of the here presented study, it should be noted in any case that

additional investigations are needed to better quantify the effects of embedding a metal insert in a laminated glass component. The complete results of the scattered-light polariscope measurements are provided in Annex II, for information and further interpretation, but are for the sake of brevity not further analysed in the current publication.

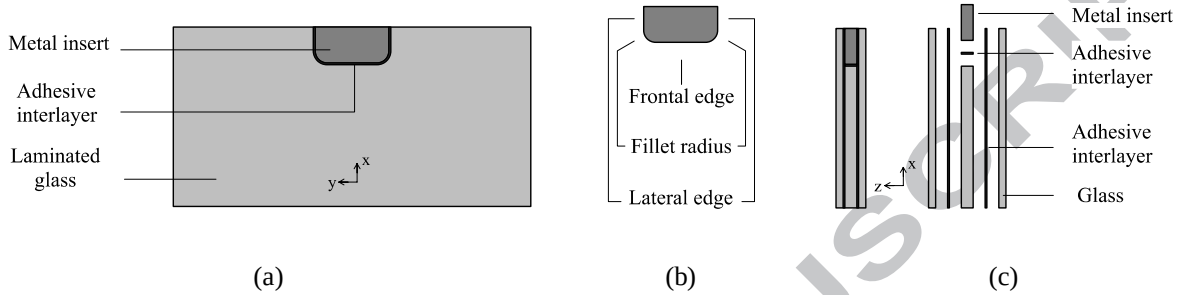

Figure 1. Schematic representation of thick embedded laminated connections (S0 series). (a) Front view, with (b) detail of the metal insert and (c) lateral view

3. Small-scale experiments

3.1. Test methods

In order to assess the mechanical performance of the so assembled connections, a set of pull-out tests was carried out at EPFL Lausanne (CH). All the laminated connections were tested by using a universal tensile testing machine, equipped with a climatic chamber (with a of range -30 to +80°C with a measurement accuracy of ±0.1°C).

The full experimental program included 12 experiments. Tests were performed at a constant temperature and in displacement control condition (with a displacement rate of 1mm/min). Four temperature levels were investigated, including experiments at 20°C, 40°C, 50°C and 60°C (with three test repetitions for each temperature).

Given the reference specimen of Figure 1, through the typical experiment, the metal insert was pulled out of the laminated pane by using a pinned connection, rigidly fixed to the testing machine. To this aim, the glass plate was also clamped to a stiff metal base, by means of two steel brackets directly connected to the base (Figures 2(b), 2(c) and 3). A 3mm slot was also machined at the base and in the brackets, to ensure a symmetric placement of the specimen. Soft aluminium plates were then placed in the slots (i.e. at the interface between the glass layers and the metal setup) to avoid glass failure due to hard contact stress intensifications. Four Linear Variable Displacement Transducers (LVDTs, i.e. two for each side), were finally used to measure the metal insert-glass panel relative displacements. The use of four LVDTs was suggested to compensate any possible rotation occurring due to fabrication

tolerances. Two video cameras were also installed inside the climatic chamber, one on each side of the specimen (see Figure 3). The overall performance of the examined connections was hence continuously video-recorded during all tests.

Regarding the temperature control and measurement during the full experimental program, a total number of four thermo-couples was used to measure the temperature before and during the tests. Past exploratory investigations have shown in fact that the heating rate of air and specimens are quite different. In addition, the sensitivity of the SG adhesive to temperature is well known to have a crucial role in the measured test results. The first thermocouple was placed directly on the specimen, the second on the setup, the third within the SG foils of the reference connection (also in the climatic chamber), while the last one was used to monitor the air temperature inside the climatic chamber. After the installation of each specimen, tests were started 30 minutes after that all thermocouples have measured the targeted temperature (within the tolerance of ±0.25°C). Temperature, load and displacement data were hence acquired with a frequency of 10Hz.

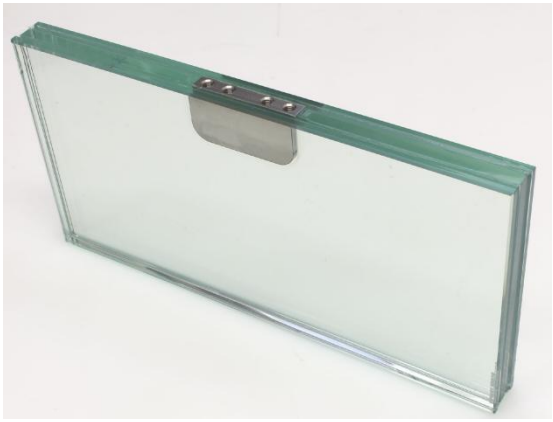

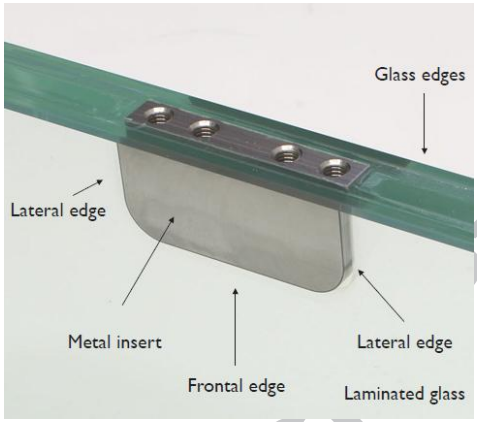

(a)

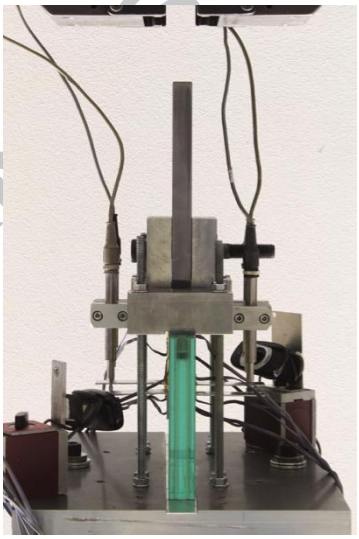

(b) (c)

Figure 2. Photo of (a) the embedded connection specimen, with (b) lateral view and (c) frontal view of the test setup.

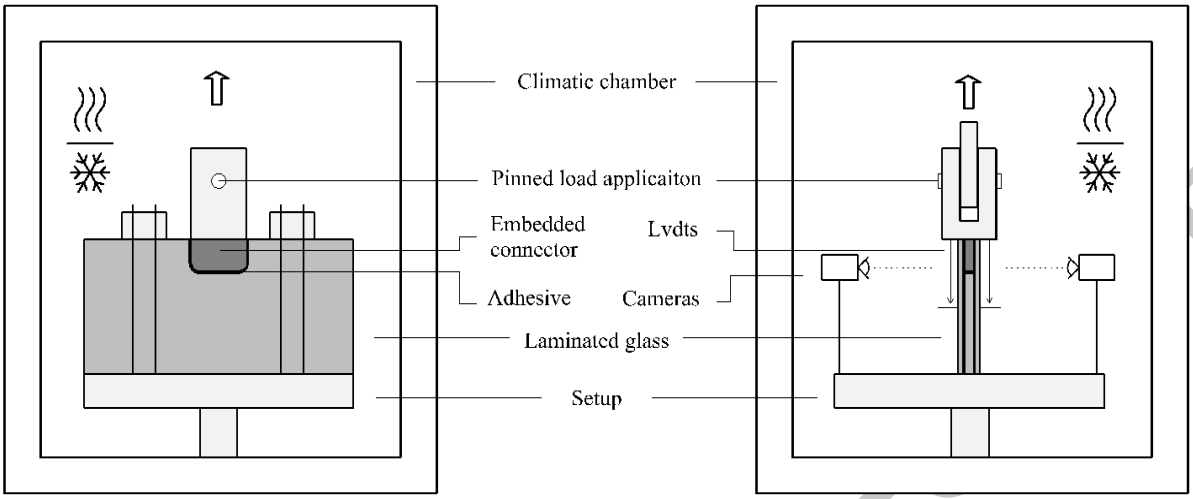

Figure 3. Scheme of the test setup for embedded laminated connections tested at different temperatures

3.2. Test results

3.2.1. Load-displacement response and maximum loading capacity

A preliminary analysis of experimental results was carried out by comparing the overall load-displacement measurements collected for each test series. These results are graphically collected in Figure 4 (a), and divided by temperature levels (separate experimental plots are also collected in Annex I). The typical load-displacement curve is characterized by an initial linear response, which is mostly dependent on the imposed temperature regime (i.e. slope reduction with temperature increase). After the initial linear stage that can be detected in the typical connection response, the experiments gave insight into to overall pull-out behaviour as well as the associated failure modes, which are both strictly related to the temperature condition. Firstly, it can be qualitatively noticed in Figure 4 that the maximum load taken up by each connection decreases when the temperature increases. At the same time, the maximum achieved displacement increases with temperature. Such a mechanical behaviour can be explained by considering the intrinsic material properties and their relation with temperature. At high temperatures, it is in fact known that the interlayer yields and develops large plastic deformations [23]. Such a phenomenon hence prevents glass fracture and manifests in high ductility for the tested connections. This is not the case for room temperature conditions, where the glass panels fail first and the collapse of the examined connections can be associated to a typically brittle collapse mechanism.

More in detail, with reference to Figure 4(a), it is possible to notice that the connections tested at 20°C demonstrated a mostly linear load-displacement curve, up to failure (with ≈56kN the average collapse load and 0.2-0.3mm the ultimate displacement). The failure configuration of such specimens

proved to occur due to glass fracture on both outer glass plies, without any kind of plastic deformation (see also Table 1).

Given the experimental load-displacement measurements collected in Figure 4, the elastic response of connections at room temperature was associated to an average axial stiffness (i.e. slope of experimental load-displacement plots) in the order of ≈220kN/mm.

For the connection at 40°C, the specimens offered a linear response up to ≈15kN, with elastic stiffness in close correlation with room temperature measurements, but followed by a load-displacement curve giving evidence of marked plastic deformations. The specimens proved to sustain maximum loads up to ≈27kN, glass fracture finally lead the specimens to collapse.

For both the testing scenarios at 50°C and 60°C, a limited linear stage response was observed (with ≈5-10kN the maximum load carried out in the elastic phase), with a mostly plastic response of the specimens. Maximum loads in the range of ≈15kN and ≈10kN were measured at 50° and 60°C respectively. Differing from tests at 20° and 40°C, glass failure was not noticed at collapse, but the interlayer foils yielding lead to large deformations of the connections (with maximum measured displacements up to ≈3mm and ≈5mm respectively).

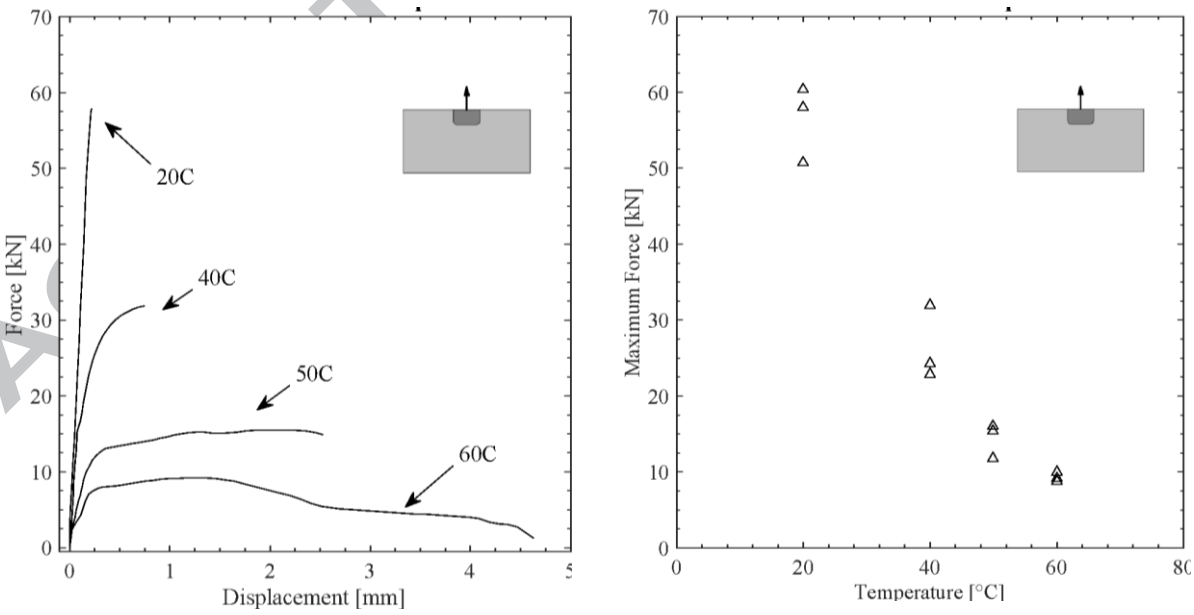

(a) (b)

Figure 4. Experimental results on small-scale thick embedded connections at different temperatures.

(a) Load-displacement curves and (b) maximum force, as a function of the imposed temperature.

Table 1. Qualitative experimental comparison on the mechanical performance of thick embedded connections at different temperatures

	T [°C]			
	20	40	50	60
Overall behaviour	Linear elastic	Linear elastic + plastic	Linear elastic + plastic	Linear elastic + plastic
SG yielding	No	Yes	Yes	Yes
Glass failure	Yes	Yes	No	No
Glass failure initiation	Outer panel (frontal embedded edge)	Outer panel (frontal embedded edge)	-	-

Temperature proved to strongly affect the maximum loading capacity of the examined connections, see Figure 4(b). In particular, it was shown that the average connection resistance F_{max} drastically reduces with temperature, especially up to 50°C, with an overall (F_{max}, T) correlation well represented by a linear fitting curve (within the tested range of termperatures):

$$F_{\max} \approx 78 - 1.2T \quad \text{(kN, °C)} \qquad (1)$$

Such an observation is in line with test expectations, as well as with earlier test results and investigations carried out on SG samples under uniaxial [23], pure tensile loading [24] and pure shear loading [25] respectively. There, the resistance of the adhesive material was in fact observed to follow a decreasing path, with the increase of temperature. From Figure 4(b) and Table 2, it can be observed that the standard deviation of experimentally measured Fmax values is sensitive to temperature variations, with larger standard deviations at room temperature than at high temperatures. This finding could be rationally related to the corresponding failure mechanisms, being low temperatures dominated by glass breakage. The latter is indeed characterized by very large statistical spread distribution.

Table 2. Maximum force of embedded connections at different temperatures

	T [°C]			
	20	40	50	60
Mean [kN]	56.40	26.34	14.44	9.35
St.dev [kN]	5.05	4.85	2.38	0.62

3.2.2. Glass cracking

Further comparative observations were finally derived from crack initiation and propagation in glass, for the full experimental program. For the 20°C and 40°C tests manifesting glass breakage, in particular, despite their rather different load-displacement responses collected in Figure 4(a), close correlation was observed in terms of failure configuration.

The final glass fracture, in particular, was usually noticed to occur in the outer glass panels composing the specimens. Glass fracture initiated - in most cases - in the region close to the edge of the metal insert, and more specifically along the embedded frontal edge. From the so detected fracture initiation point, the fracture in glass propagated then orthogonally to the pull-out loading direction, i.e. along the long edge of the metal insert. In a subsequent stage only, the cracks were then observed to deviate and propagate towards the supports of the specimens. Figure 5(a) shows the typical crack pattern for an embedded connection specimen at the end of the test (20° and 40°C).

In the case of experiments at high temperatures, a different failure configuration was observed. In particular, the absence of glass fracture gave evidence instead of several bubbles, appearing within the adhesive layers (see Figure 5(b)), that is in line with the earlier investigation results reported in [25]. Such bubbles mostly appeared and propagated at the end of the linear response stage of the load-displacement curve, i.e. in the first plastic stage. In terms of damage location in the specimens, these bubbles were generally located at the interface between the frontal edge of the metal insert and the edge of the inner glass plate (see also section 4).

(a)

(b)

Figure 5. Final collapse configuration for thick embedded connections, as observed (a) due to glass cracking at 20° and 40°C (frontal view), or (b) due to adhesive yielding at 50° and 60°C (detail).

4. Numerical and analytical investigation

Following section 3, the experimental study was further extended by means of Finite Element numerical models and analytical studies, aimed to further support and clarify the test observations.

4.1. Finite Element numerical model

A Finite Element numerical model representative of the typical small-scale embedded connection specimen was first realized in ABAQUS [17]. In doing so, careful consideration was attributed to the geometrical and mechanical description of the specimens components, as well as for the description of

the pull-out experimental setup. Displacement-controlled simulations were carried out in ABAQUS/Explicit, in the form of dynamic analyses with quasi-static increase of imposed displacements.

Due to symmetry, half the reference specimen only was described, by taking into account their longitudinal plane of symmetry (see Figure 6). Nominal dimensions were taken into account for all the specimen components. Appropriate boundary conditions were hence considered, along the mid section of the laminated glass panel. The tensile load was indeed described in the form of a linear increasing vertical displacement, being uniformly imposed to the top face of the metal insert.

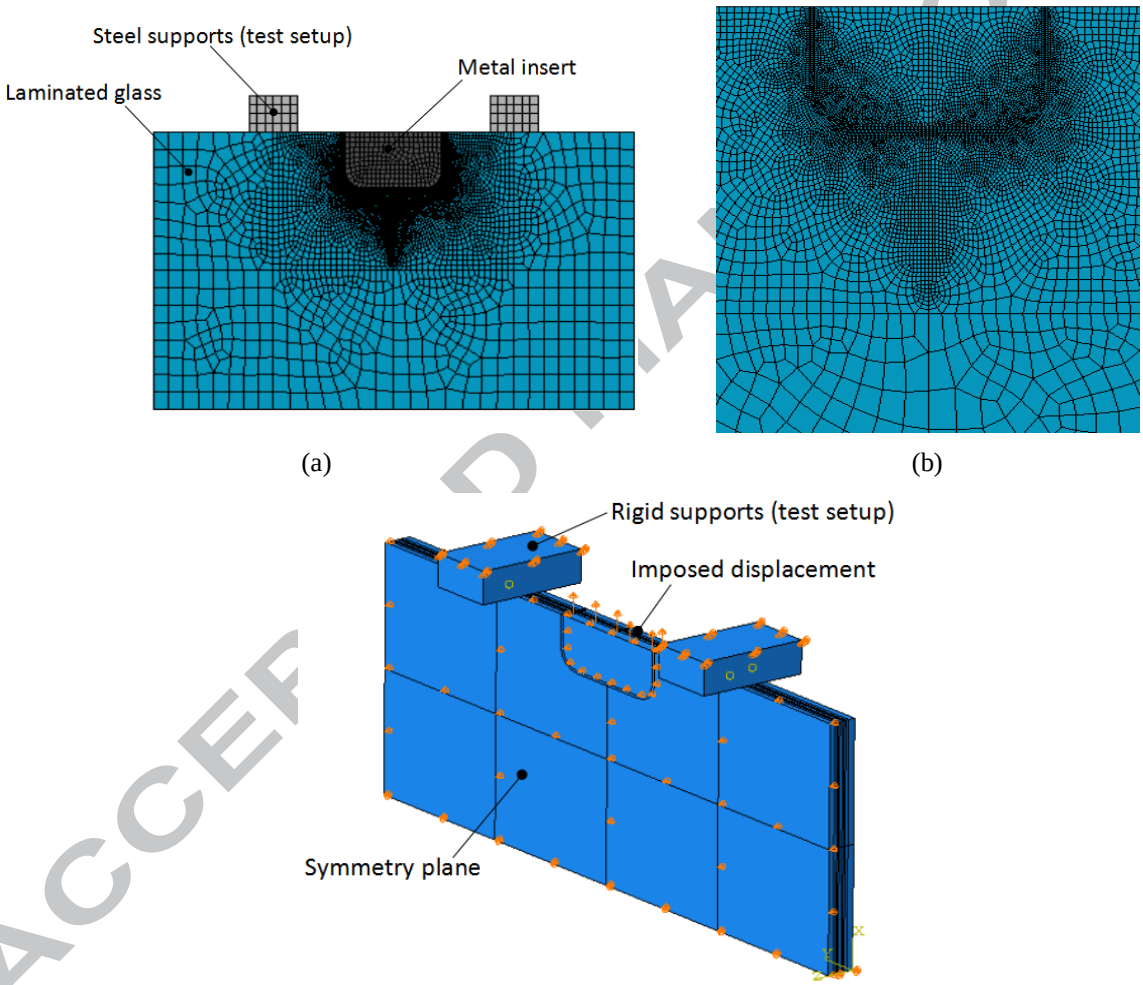

Figure 6 . Reference FE model for thick embedded connections (ABAQUS).

(a) Frontal view, with evidence of mesh pattern, and (b) mesh detail (in evidence, the glass components only), with (c) boundaries.

Aiming to ensure the accuracy of global and local estimations and stress distributions, solid elements were used to describe the specimen geometry. A set of 8-node solid brick elements (C3D8R type) was taken into account for (i) the metal insert, (ii) the SG foils and (iii) the glass layers. The (i)-to-(iii) specimen components were assumed to be rigidly connected, hence - as also in accordance with earlier numerical studies on structural glass composites and assemblies (i.e. [26], [27]) - possible debonding effects were fully disregarded at this stage of the research study. In this regard, the reliability of FE results is limited to connection loading configurations in which glass breakage is representative of the major reason of collapse (i.e. room and medium temperatures, up to 30°-40°C). Additional FE efforts should be indeed required at high temperatures, where yielding of the adhesive as well as possible debonding phenomena could also manifest (i.e. including cohesive damage interactions, etc.), see section 5. In addition to the (i)-to-(iii) model components, further solid brick elements were then used to describe the test setup, so to ensure the same loading and boundary configuration of the experimental tests (see Figure 6). For the latter components, being assumed to consist of stainless steel, *surface-to-surface* contact interactions were defined at the interface with the laminated glass panel, so to allow frictionless relative tangential displacements (*penalty* method), as well as a *"hard normal"* contact behaviour in the direction of the imposed displacement (i.e. possible separation of the surfaces in contact, in presence of tensile loads, but penetration prevented in presence of compressive reaction forces).

Globally, the mesh pattern and size was chosen so that reliable predictions on crack propagation in the glass panels could be obtained, for the examined loading configuration. Following the experimental observations at failure, a free mesh scheme was adopted, with a fine mesh size close to the metal insert (0.2mm the reference size of brick elements), while a coarse mesh size was defined at the end of glass plates (12mm the maximum assigned element size). The final assembly consisted of 68,000 solid elements and 235,000 degrees of freedom.

Careful consideration was paid for materials, including tensile cracking of glass and the non-linear behaviour of the adhesive material. In the case of float glass, in particular, the concrete damaged plasticity ('CDP') material model was used [17], see Figure 7. In accordance with material product standards [18], the nominal characteristic tensile strength σ_{tk}=45MPa was taken into account, with reference nominal values also for modulus of elasticity (E_{glass}=70GPa) and Poisson ratio (ν_{glass}=0.23). Any residual stresses field is neglected in the numerical analysis. In terms of compressive resistance, a conventional value σ_{ck}=1000MPa [28] was indeed considered, as also in accordance with the numerical investigation proposed in [26][29]. The CDP damage model (see the ABAQUS Theory Manual for an extended theoretical background [17]), describes the inelastic compressive and tensile behaviours of a given brittle material in the form of a multi-hardening plasticity and a scalar isotropic damaged elasticity characteristic curves (Figure 7).

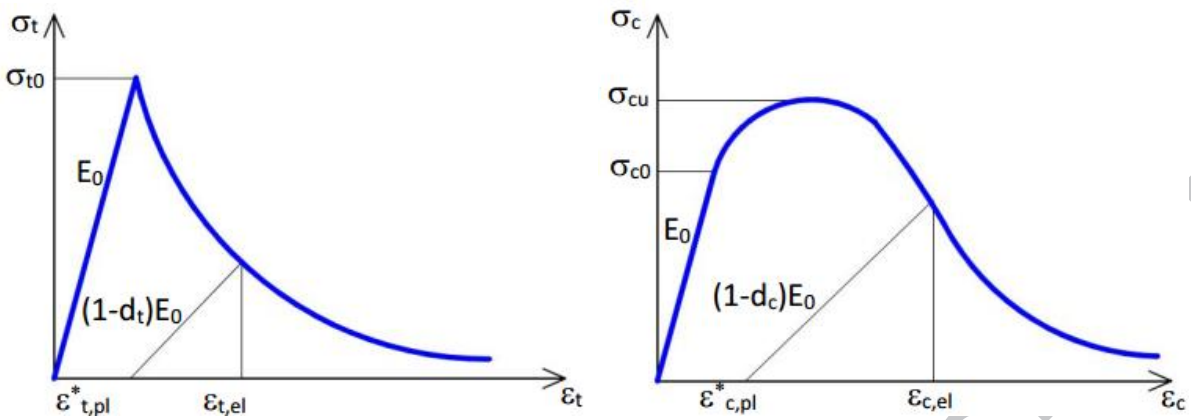

(a) (b)

Figure 7. Mechanical constitutive laws for the CDP model representative of (a) tension and (b) compression behaviours (ABAQUS). Input parameters derived from [26, 29].

In this study, the main post-cracked input parameters were defined in accordance with earlier research contributions as well as literature references (see also [26][29]), so to account for the brittle behaviour of glass. In doing so, to avoid additional numerical instabilities for the post-cracked stage predictions, the physical deletion of cracked shell elements from the mesh pattern was then fully disregarded. As such, failed glass elements with almost null residual stiffness and strength were not removed from the 3D assembly. In terms of post-processing of the obtained FE data, material degradation (SDEG) due to cracking was monitored to detect glass breakage, together with stress evolution and distribution.

For SentryGlas®, as also in accordance with [23], a non-linear stress-strain constitutive law was taken into account, including a modulus of elasticity of E_{SG}=120MPa and a Poisson' ratio equal to ν_{SG}=0.49, as well as a yielding stress in the order of 20MPa.

For the metal insert, finally, an elasto-plastic material behaviour was defined to describe 316L features, with E_{steel}=193GPa, ν_{steel}=0.3, 200MPa and 500MPa respectively the yielding and ultimate stress.

4.2. Numerical assessment of test results

Given the reference model described in section 4.1, qualitative and quantitative comparisons with experimental observations at room temperature were first carried out.

The FE specimen representative of the reference connection exhibits a linear elastic load-displacement response, up to the first attainment of the characteristic tensile resistance of glass σ_{tk}. Taking advantage of the input material constitutive laws and damage models recalled in section 4.1, the

initiation and propagation of cracks in glass were hence numerically monitored as a function of the imposed displacement, and compared to test observations for the specimens at collapse.

Figures 8-to-11, in this regard, collect some major outcomes of the FE analyses.

Figures 8(a) and (b), in particular, give evidence that the stress field distribution in the examined connections is rather complex. The principal stress field is in fact non-uniform through the thickness of glass panels and on the specimens dimensions, and exhibits large gradients in all the three dimensions. Important stress variations are indeed observed both (i) in-plane (i.e. x and y-axes) and (ii) through the thickness (i.e. z-axes), due to several reasons. The in-plane stress field distribution is non-uniform because the pull-out force is firstly transferred to a local overlapping region and only then it diffuses over the glass panel by adhesive shear stresses. The non-uniform stress distribution through thickness is instead related to the eccentricity of the resulting force, at the level of the metal insert. This is due to the eccentricity between the pull-out force applied to the metal insert and the resulting forces in the glass panels.

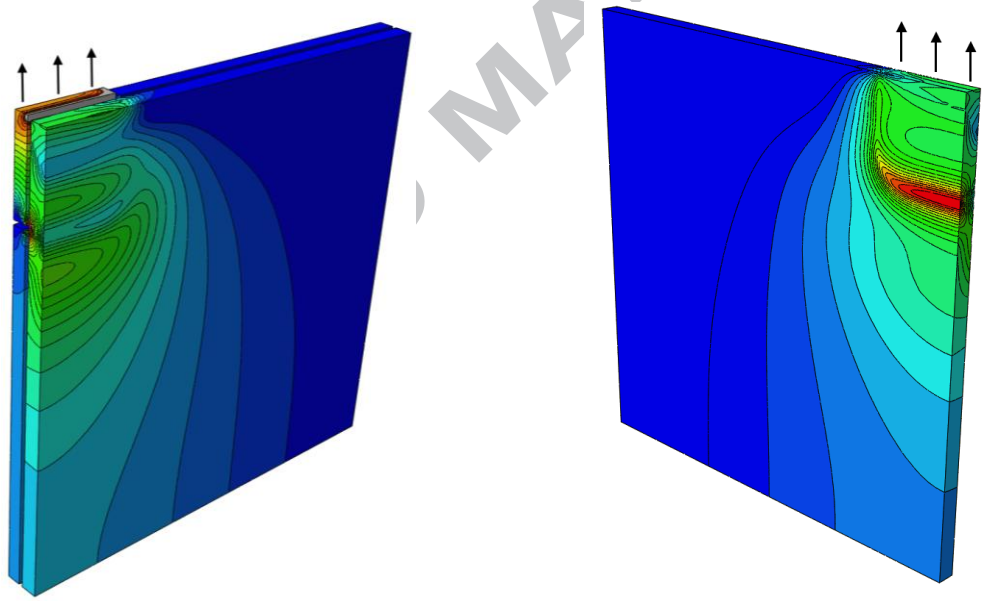

(a) (b)

Figure 8. Field distribution of maximum principal stresses in the thick embedded connection under pull-out force: (a) external face and (b) internal face of the outer glass ply.

Given the experimental load-displacement measurements collected in Figure 4(a) and the FE predictions here summarized, some interesting correlations were found between them. In Figure 9, for example, a comparative plot is proposed, with evidence of three experimental measurements for the set of specimens at room temperature, with the corresponding FE estimations. Rather close correlation

can be noticed in terms of elastic stiffness, with numerical and average experimental values in the order of 250kN/mm and 220kN/mm (193-277kN/mm the range of variation) respectively.

First glass cracking was numerically observed to clearly manifest at a maximum load of ≈40kN (≈0.15mm the corresponding displacement), see also Figure 11. Later on, cracks rapidly propagated in the glass panels, leading the connection to collapse with a maximum load bearing capacity of ≈62kN (≈0.6mm the measured displacement). Through the cracking phase, a marked reduction of the specimen' stiffness was numerically observed (≈110kN/mm, which corresponds to a 50% reduction in elastic stiffness). Given the well-known scatter in glass mechanical properties [1, 2] as well as possible uncertainties in the glass-to-metal adhesion for all the specimens components and the FE modelling assumptions described in section 4.1, at the current stage of the research, the comparisons proposed in Figure 9 can be considered satisfactory and well representative of the actual mechanical performance of the examined connections.

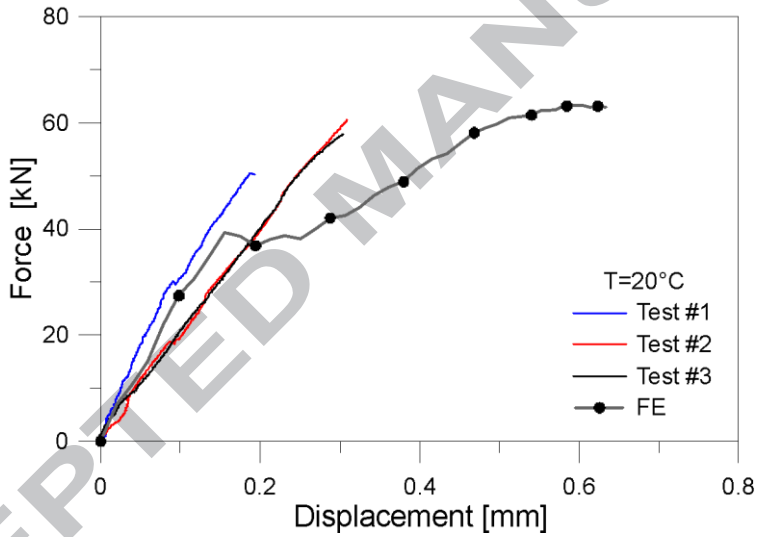

Figure 9. Experimental and numerical load-displacement curves for the thick embedded connections at room temperature.

Globally, the predictions of the numerical model proved in fact to match the experimental observations at different levels. Firstly, the numerical results show that at room temperature the final glass fracture is expected to occur in the outer glass plies. This is confirmed by the experimental observation since the maximum force at room temperature is dominated by glass fracture, the latter located in the two outer plies. Then, the numerical model indicates that glass failure should occur close to the edge of the embedded metal insert, namely along the frontal edge. This is also confirmed by the experimental observation since the glass breakage is located at the level of the frontal insert edge, where the stress field obtained from the model exhibits higher intensification. Finally, through thickness, it is predicted that the glass breakage of the external ply initiates at the inner surface rather

than at the external ply. In this regard, Figure 10 collects two photos through the thickness of the broken specimen, after testing. There, the initiation of glass failure is indicated with a circle and it is clearly located at the inner surface of the outer ply.

(a) (b)

Figure 10. (a) Photo through thickness of the broken glass after testing: failure initiation is indicated by a circle (b) zoom view of the photo at the crack initiation.

Close correlation was finally observed between the experimental crack pattern, as can be seen from a comparison between the experimental results in Figure 5(a) and the corresponding FE results in Figure 11.

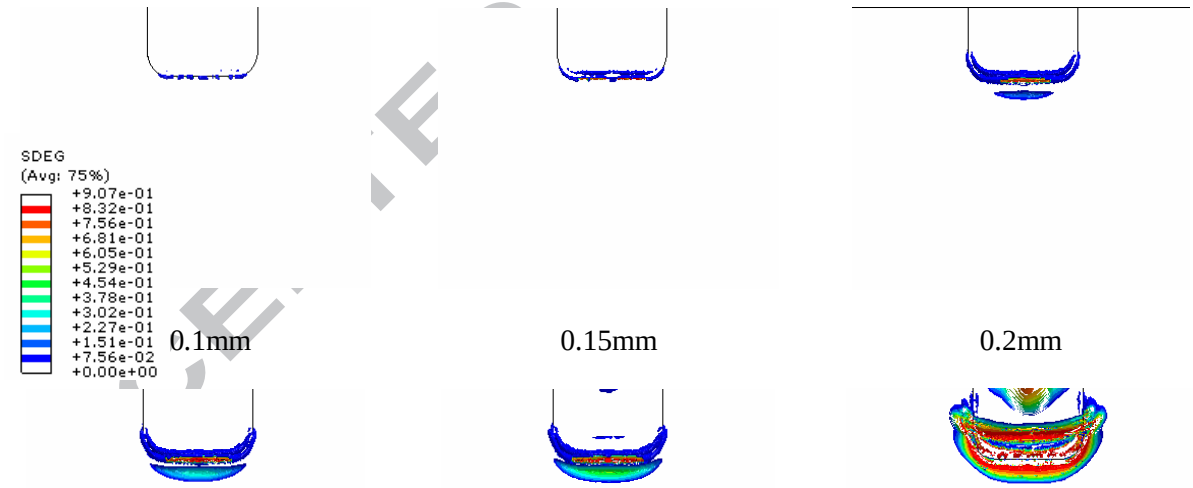

Figure 11. Progressive crack initiation and propagation in glass (frontal view), as a function of the imposed displacement (ABAQUS).

4.3. Resisting mechanism

Following section 4.2, in order to better explain the mechanical behaviour of embedded connections and to interpret the stress distribution in the glass panels, the in-plane and the out-of-plane mechanism of load transfer were then separately analysed more in detail.

The transversal mechanism of load transfer can be rationally explained by the scheme proposed in Figure 12(a). The load is firstly applied to the metal insert, which then transfers the force to the outer glass ply. Because of the eccentricity between the metal insert and the outer glass ply, the latter is subjected to tensile force plus momentum. These force and momentum have to be equilibrated by the stresses in the glass, as indicated by the scheme of Figure 12. This motivates the non-uniformity of stresses in the outer ply. More in detail, it explains why the stresses at the internal face of the outer ply are higher than the stresses at the external face of the outer ply. Especially close to the frontal edge of the metal insert high stress intensification occurs in the outer ply. In the scheme of Figure 12 the element with maximum tensile stress is indicated with a dashed line. It can be observed that this consideration is in agreement with the location of the crack initiation observed in the test and with the results of the numerical model.

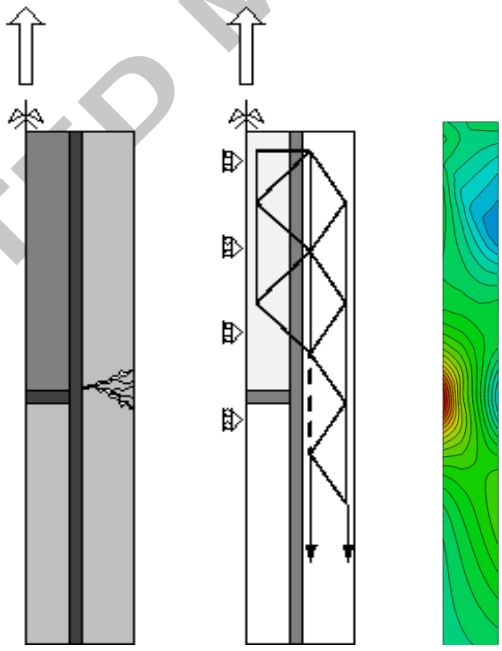

Figure 12. Mechanical model for the transversal resisting mechanism of thick embedded connections (transversal cross-section). (a-b) Scheme of the load transfer mechanism and (c) corresponding stress field distribution, as obtained from the FE numerical model (ABAQUS).

The in-plane mechanism of load transfer is indeed explained by the scheme of Figure 13. Along the metal insert, the load is vertically transferred from the insert to the glass panel. On the right side and left side of the metal insert the direction of load transfer is inclined with respect to the vertical direction, as indicated by Figure 13(a). This is because the applied force has to diffuse over the width of the specimen. The compressive elements that equilibrate the tensile one are then indicated in Figure 13(a) by a double-arrowed line. In brittle material the crack plane is usually located orthogonal to the maximum principal (tensile) direction. Accordingly, the crack is expected to occur along the direction of the minimum principal, since by definition they are orthogonal to the maximum one. The comparison of Figure 13(a) with Figure 13 (b) and Figure 5 shows that these analyses are in line with the results of numerical model and with the experimental observations.

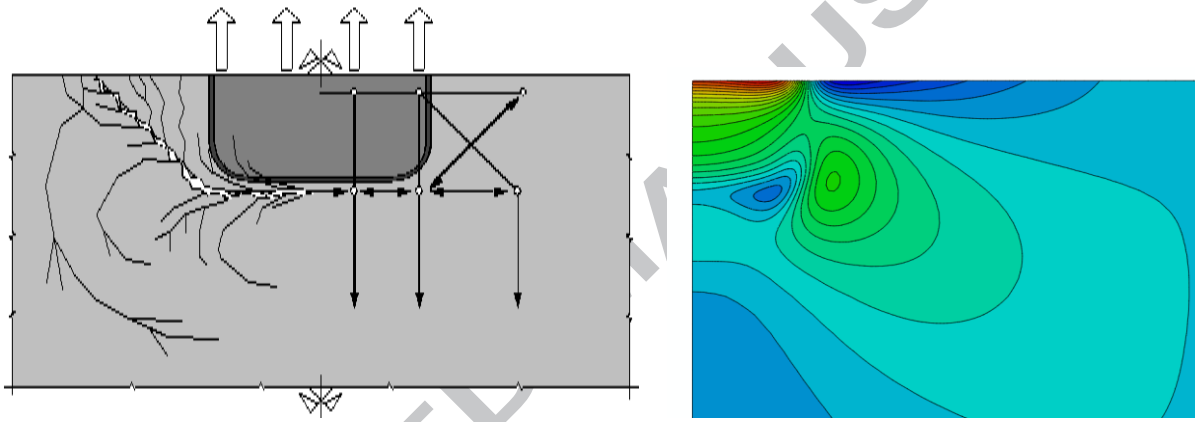

(a) (b)

Figure 13. Mechanical model for the in-plane resisting mechanism of thick embedded connections (frontal view). (a) Scheme of the load transfer mechanism and (b) corresponding $_y$ stress field distribution, as obtained from the FE numerical model (ABAQUS).

Given major outcomes briefly summarized in Figures 12 and 13, a conservative design equation can be proposed to estimate the stress in the outer glass panel, given an applied tensile load F see Eq.(2):

$$\sigma_x = \frac{F}{t_1 \cdot B_{eff}} \cdot \left(0.5 + 1.5 \frac{(t_1 + t_2)}{t_1}\right) \quad (2)$$

There, t_1 and t_2 denote the thickness of the outer glass plies and the metal insert, respectively. The parameter B_{eff} represents then an equivalent width for the embedded connection, able to account for the three-dimensional stress distribution. In particular, B_{eff} is intended to describe the stress diffusion along each direction, from the metal insert towards the glass plies. Future work should focus on a extensive numerical parametrical study to calibrate B_{eff}. More in details, such parameter has to be

calibrated by three-dimensional FE non-linear modelling of the examined connection typology, for different values of thicknesses t_1, t_2 and the metal insert dimensions. Indeed, the stress distribution in the glass strongly depends on the adhesive stiffness and connection geometry.

4.4. Adhesive stress state

Following such considerations on stress distribution in the glass plies, the stress state tensor in the adhesive was hence further analysed, in order to study more in detail the phenomenon of the appearing of bubbles in the adhesive (i.e. as experimentally observed for the connections tested at high temperatures). In the investigated laminated embedded connections, the adhesive layer located between the glass panels and the metal insert is characterized by a typically high confinement state. Such a confinement has minor effects if the stress tensor is dominated by its deviatoric component. This is the case, for instance, of the adhesive located along the lateral edges of the metal insert (see Figure 14). There, the strain energy potential is in fact mainly related to material distortion. Along the frontal edge, instead, the stress state is characterized by a large hydrostatic component. There - because of the confinement state - the application of tensile stress along one direction (i.e. the loading direction, in this case) leads to normal stresses also along the other two orthogonal directions. The magnitudes of the confinement stresses depend on the confinement level and on the Poisson's ratio. This effect has been also demonstrated in [24], where analytical equations of stress tensor and stiffness - given a reference connection - were derived as a function of the geometry, confinement effect and Poisson ration. From the past mathematical expressions, it is generally possible to observe that - for adhesive materials with Poisson's ratio close to 0.5 - the stiffness tends to infinity and that the magnitudes of the confinement stresses is similar to the one of the applied stress. This implies that, with no shear stresses applied, the stress tensor is described by an almost perfect hydrostatic solicitation, as shown in more detail in [24].

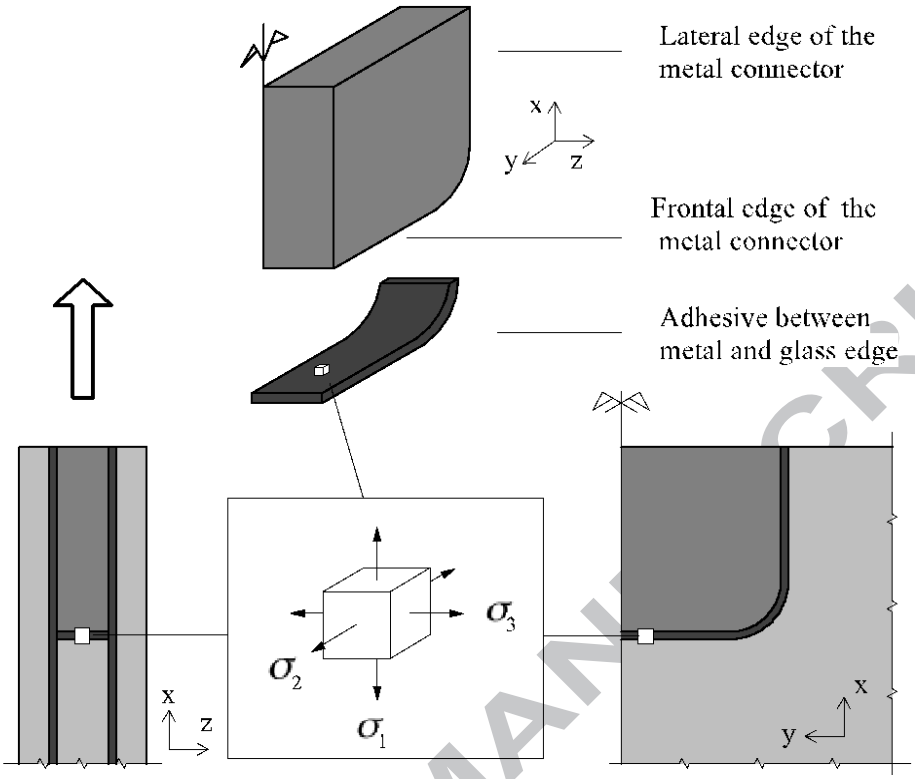

Figure 14. Typical stress state for the adhesive at the frontal edge in thick embedded connections.

The general considerations briefly described above to emphasize the adhesive confinement and the stress tensor effects, in accordance with [24], were further confirmed in the current research by FE results of three-dimensional numerical modeling. Figure 15(a), in this regard, shows the stress distribution in the adhesive between the metal insert and the glass panels. Namely, the hydrostatic component of the stress tensor in the adhesive it is shown. The model gives very large values of triaxiality. This indicates that the confinement stresses are in the same order of magnitude of the applied stresses. Given the Poisson's ratio of the SG close to 0.5 [23][25], this is in agreement with the analytical consideration stated above.

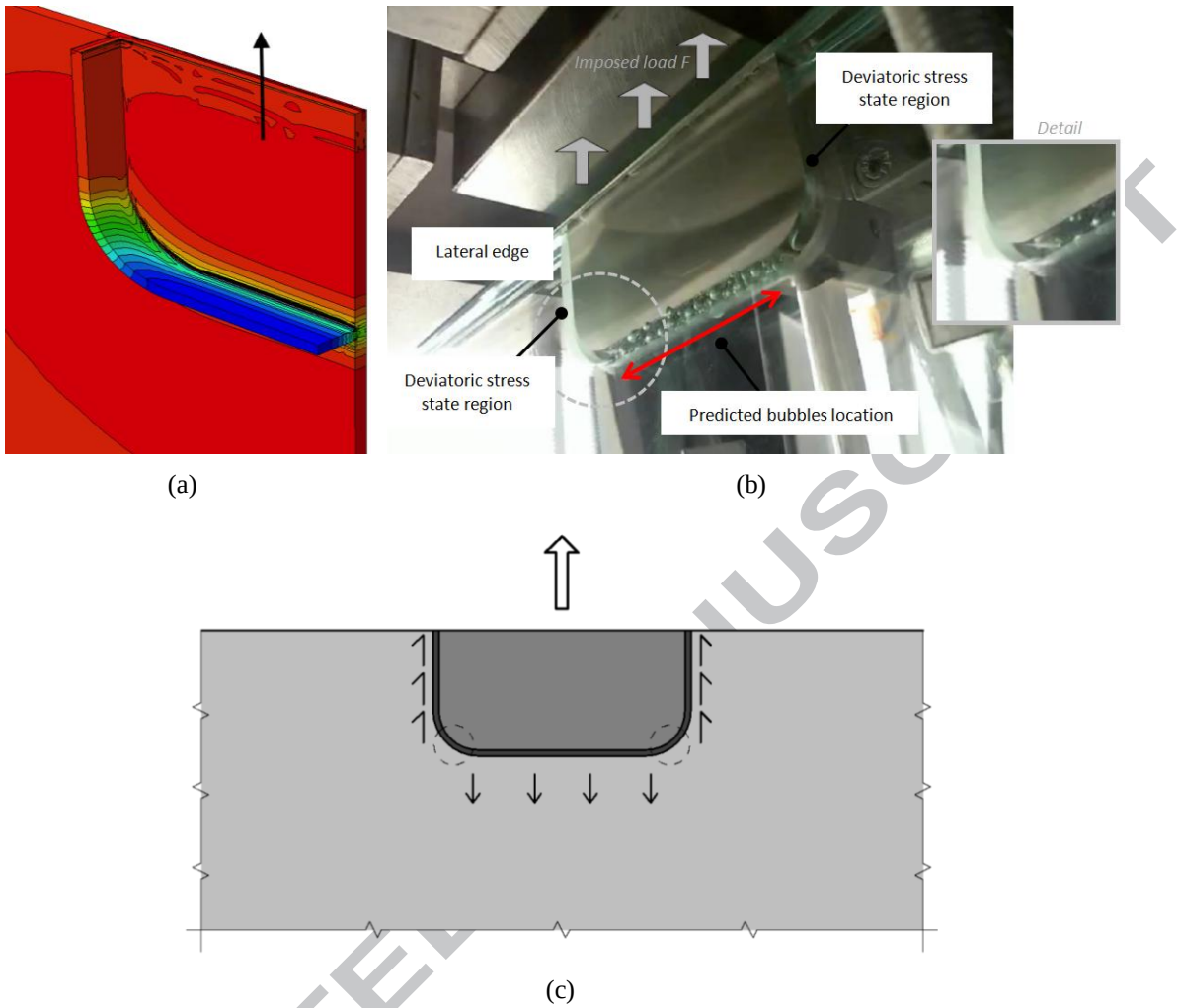

Figure 15. Comparison of the (a) field distribution of the hydrostatic component of the stress tensor in the adhesive layer (ABAQUS, with glass panels and metal insert hidden from view), with (b) the experimental observation for connections tested at high temperature (in evidence, the bubbles). (c) Schematic representation (frontal view) of the typical stress distribution in the adhesive, at the frontal and lateral edges of the metal insert.

One of the major findings of the past study discussed in [24] is then that the SG adhesive, when subjected to large hydrostatic state at high temperature, exhibits a cohesively propagation of bubbles (i.e. more and more bubbles appear within the adhesive layer). This phenomenon, in particular has been observed by means of experimental investigations on circular SG laminated connections under pure tensile loading. There, the stresses state of the adhesive is in fact typically characterized by an high hydrostatic component, as in the case of embedded connections (i.e. at the edge). As a direct effect, (a) large hydrostatic stress states correspond to potential strain energy mainly dominated by volume changes. However, at the same time, (b) the material has a Poisson's ratio value close to 0.5, hence almost no volume change is allowed. Both the (a)-(b) conditions can be satisfied only by the

creation of voids bubble. Consequently, according to the results of [24] as well as to the numerical and analytical results earlier discussed in this paper, it is expected that also embedded laminated connections exhibit bubbles in the adhesive (i.e. at the interface between the metal insert and the glass edges). Such considerations and general observations proved to find validation in the experimental tests. During the experiments at high temperature (>40°C), bubbles similar to observations reported in [24] were in fact noticed to appear in the embedded connections (see Figure 15(b)). These bubbles were found to be mainly located between the metal insert and the inner glass plate, as also in accordance with previous analytical and numerical results. More specifically, the bubbles were mostly located along the frontal edge of the metal insert. Along this edge, the propagation of bubble stops at the fillet radius (see Figure 15(c)). The reason is that at the fillet radius, the hydrostatic component of the stress tensor reduces. Deviatoric stresses start indeed to develop, since the adhesive material goes from tensile deformation to shear deformation, from the frontal to the lateral edge respectively.

5. Concise parameter study

In conclusion, the reference FE model described in section 4 ('M0' model, in the following) was further elaborated and analysed, aimed to preliminary assess the effects of some key input aspects on the mechanical response of the same connection typology. Variations included adhesive connection details as well as material mechanical properties.

In the first case, for example, the effect of a fully rigid glass-to-metal connection on the whole contact surfaces (i.e. being representative of an upper ideal condition for so assembled thick embedded connections) was compared with a FE specimen ('M1', see Figure 16) representative of a lower limit condition for the same specimen. In doing so, the inner glass ply was in fact disconnected from the metal insert, as in the case of possible lack of adhesion could occur during the production process.

The overall effect of such a connection detailing proved to have important effects on the response of embedded connections, see Figure 16(b). In particular, a rather brittle elastic performance was observed for the specimen, with maximum resistance up to ≈56kN and in close correlation with average experimental measurements, as well as with limited variations from the M0 estimations. Major effects were indeed noticed in terms of elastic stiffness of the same connection, with marked reduction compared to the M0 case (≈130kN/mm), as well as compared to the test measurements. In this regard, being the M1 configuration representative of a lower limit condition for the examined connections, it is hence assumed that the actual stiffness and ultimate resistance would be comprised between the M0 and M1 predictions. In terms of glass fracture and crack propagation, insignificant variations were in fact observed between the M0 and M1 damage scenarios (see for example Figure

11), with first glass cracks starting to manifest, in both the cases, from imposed displacements in the order of ≈0.1mm.

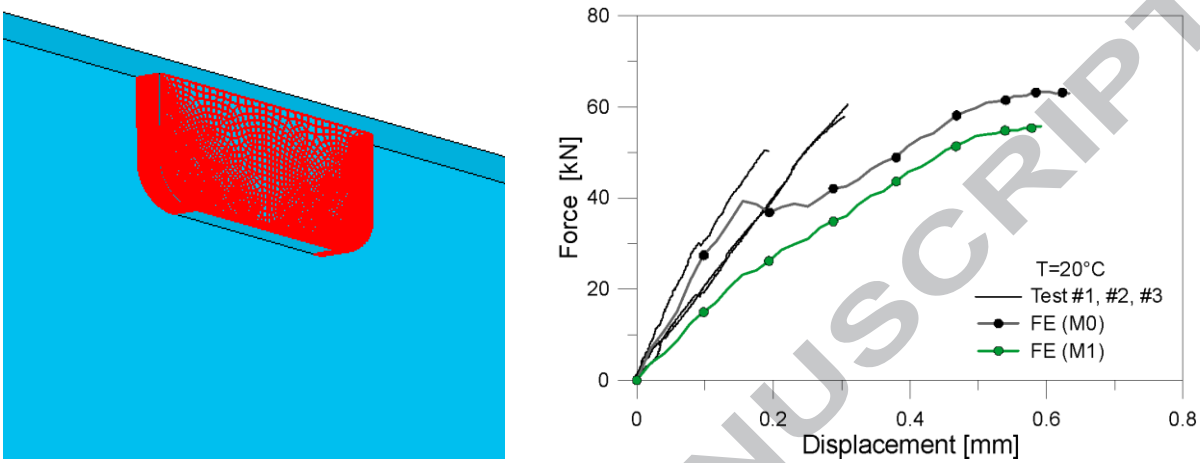

(a) (b)

Figure 16. Numerical assessment of glass-to-metal adhesion effects on the overall mechanical response of the examined thick embedded connections (ABAQUS). (a) Surface detail and (b) corresponding load-displacement curves.

Given the experimental test results discussed in [24] for SG adhesive connections under different temperature scenarios, a second set of FE simulations was carried out by modifying the SG mechanical properties of the interlayer foils, compared to the M0 model. Tensile test results presented in [24] for SG adhesive connections, in particular, showed a rather similar failure mechanism for specimens at -20°C up to 40°C, together with a rather stable SG elastic stiffness, even with progressive decrease of the corresponding resistance, with the temperature increase (≈1% from 20° to 40°C). So far, major resistance variations were observed with higher temperatures, with ≈15%, ≈35% and ≈82% resistance decrease at 50°, 60° and 80°C respectively. In this research study, the FE reference M0 model was hence modified, by accounting for the SG mechanical properties derived from [23]. Comparative results are summarized in Table 3 and Figure 17, as obtained from the modelling assumptions described in section 4. Despite rather interesting correlation was noticed between qualitative experimental observations and corresponding FE models (see Tables 1 and 3), the same simulations further confirmed the occurrence of delamination and local adhesive effects that the actual FE models are not able to capture, hence resulting in overestimated mechanical responses for the same connections at high temperatures, hence suggesting the need for further investigations.

Table 3. Qualitative numerical comparison on the mechanical performance of thick embedded connections at different temperatures

	T [°C]				
	20	40	50	60	80
SG yielding	No	Yes	Yes	Yes	Yes
Glass fracture	Yes	Yes	Yes (minor local cracks)	Yes (minor local cracks)	No
Glass fracture initiation	Outer panel (frontal embedded edge)	Outer panel (frontal embedded edge)	Outer panel (frontal embedded edge)	Outer panel (frontal embedded edge)	-

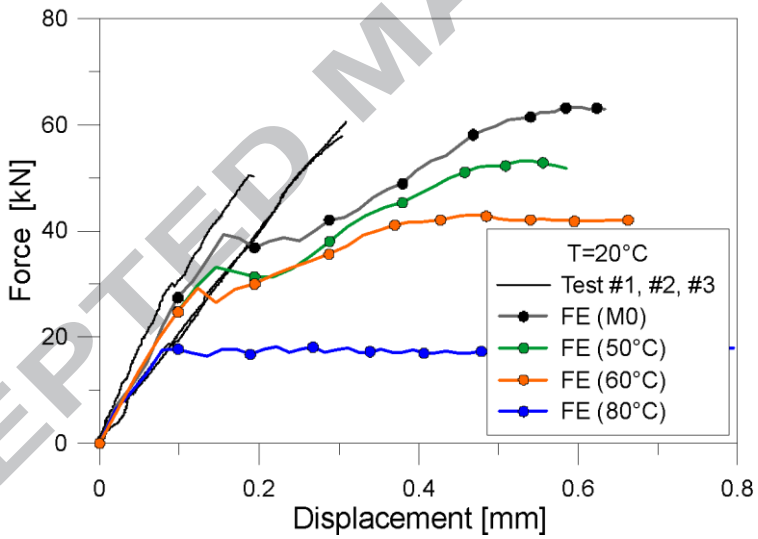

Figure 17. Numerical assessment of adhesive sensitivity to temperature variations, on the overall mechanical response of the examined thick embedded connections (ABAQUS).

6. Summary and conclusion

In this study, the mechanical behaviour of embedded laminated connections was investigated by means of experimental tests and numerical/analytical models. Firstly, the results of experimental investigations at different temperatures were presented, giving evidence of major effects of several

temperature conditions on the actual load bearing capacity and failure mode of the examined connection typology. It was in fact observed that temperature markedly affects not only the maximum load carrying capacity, but also the failure mode.

In order to further explore the experimental findings, the results of non-linear numerical model and analytical considerations were then used to properly understand the response and the different failure modes of embedded connections. Namely, it was observed that the modelling predictions are in agreement with the stress distribution, location of glass fracture, and the comparison of bubble in the adhesive observed during the test. Due to FE modelling assumptions at the current stage of the research investigation, this is especially true as far as low-medium temperatures are not exceeded, i.e. as far as debonding phenomena are not prevalent on the collapse mechanism of the same connections.

In this regard, further preliminary sensitivity analyses were also briefly presented, giving evidence of major influencing parameters on the overall performance of thick embedded connections.

Acknowledgments

The authors would like to thank the SNSF for founding the present research (Grants 200020_150152 and 200021_134507) and Nuova Oxidal for the support in the production of metal components. In addition, the contribution of Elodie Vermot and Leda Calgeer to the experimental testing is gratefully acknowledged.

Finally, both the European COST Action TU0905 “Structural Glass” (2010-2014) and the currently ongoing COST Action TU1403 “Adaptive facades network” (2014-2018) are acknowledged for facilitating networking between the involved researchers.

References

[1] M Haldimann, A Luible, M Overend (2008). Structural use of glass. IABSE, ISBN 978-3-85748-119-2

[2] M Feldmann, R Kasper, B Abeln, P Cruz, J Belis, J Beyer, et al (2014). Guidance for European Structural design of glass components – support to the implementation, harmonization and further development of the Eurocodes. Report EUR 26439, Joint Research Centre–Institute for the Protection and Security of the Citizen, doi: 10.2788/5523, Pinto Dimova, Denton Feldmann (Eds.)

[3] L. Blandini, "Structural Use of Adhesive in Glass Shells," Thesis Dissertation, University of Stuttgart, 2005

[4] D. Callewaert, A. Van Hulle, J. Belis, F. Bos, J. Dispersyn, and B. Out, "The problem of a failure criterion for glass-metal adhesive bonds," in *Glass Performance Days*, 2011

[5] J. Dispersyn, M. Santarsiero, J. Belis, and C. Louter, "A preliminary study of the nonlinearity of adhesive point-fixings in structural glass facades .," *J. Facade Des. Eng.*, vol. 2, no. 1–2, pp. 85–107, 2014

[6] M. Netusil and M. Eliášová, "Experimental and Numerical Analysis of Glued Steel-Glass Joints," in *Challenging Glass 2*, 2010, no. May, pp. 269–276

[7] K. Machalická, M. Eliášová (2017). Adhesive joints in glass structures: effects of various materials in the connection, thickness of the adhesive layer, and ageing. *Int. J. Adhes. Adhes.*, 72: 10.22

[8] J. Belis, A. Van Hulle, D. Callewaert, and J. Dispersyn, "Experimental investigation of unconventional canopy prototypes, suspended by adhesive bonds," in *Challenging Glass 3*, 2012

[9] J. Dispersyn, S. Hertelé, W. De Waele, J. Belis (2017). Assessment of hyperelastic material models for the application of adhesive point-fixings between glass and metal. *Int. J. Adhes. Adhes.*, 77: 102-117

[10] A. Van Hulle, J. Belis, D. Callewaert, L. Scheerlinck, and B. Out, "Development of structural adhesive point-fixings," in *Glass Performance Days*, 2011

[11] M. Overend, Q. Jin, and J. Watson, "The selection and performance of adhesives for a steel–glass connection," *Int. J. Adhes. Adhes.*, vol. 31, no. 7, pp. 587–597, Jun. 2011

[12] J. O'Callaghan and G. Coult, "An all glass cube in New York City," in *Glass Performance Days*, 2007

[13] J. O'Callaghan, "Adventures with Structural Glass," in *Glass Performance Days*, 2012

[14] S. Sitte and A. Wolf, "TSSA-bonded point-supported structural glazing of insulating glass units at Dow Corning's European Distribution Center," in *Engineered Transparency*, 2012

[15] P. Carvalho and P. J. S. Cruz, "Connecting Through Reinforcement - Experimental Analysis of A Glass Connection Using Perforated Steel Plates," in *Challenging Glass 3*, 2012

[16] M. Santarsiero, P. Carvalho, C. Louter, and P. J. S. Cruz, "Experimental and numerical investigations of metal-to-glass embedded connections with thin stainless steel plate," in *COST Action TU0905, Mid-term Conference on Structural Glass*, 2013

[17] K. Puller and W. Sobek, "Load-carrying behaviour of metal inserts embedded in laminated glass," in *Challenging Glass 3*

[18] Simulia (2016). ABAQUS v.6.14 computer software and online documentation, Dassault Systems, Providence, RI, USA

[19] EN 572–2:2004. Glass in buildings-Basic soda lime silicate glass products. CEN, Brussels, Belgium

[20] SentryGlas® Ionoplast Interlayer - Technical Data Sheet, www.sentryglas.com (accessed October 2017)

[21] ASTM A666-15, Standard Specification for Annealed or Cold-Worked Austenitic Stainless Steel Sheet, Strip, Plate, and Flat Bar, ASTM International, West Conshohocken, PA, 2015, www.astm.org, DOI: 10.1520/A0666-15

[22] Aben H, Ainola L, Anton J. Integrated photoelasticity for nondestructive residual stress measurement in glass. Opt Lasers Eng 2000; 33(1):49-64. ISSN 0143-8166. doi: http://dx.doi.org/10.1016/S0143-8166(00)00018-X

[23] M. Santarsiero, C. Louter, and A. Nussbaumer, "The mechanical behaviour of SentryGlas ionomer and TSSA silicon bulk materials at different temperatures and strain rates under uniaxial tensile stress state," Glas. Struct. Eng., 2016. http://dx.doi.org/10.1007/s40940-016-0018-1

[24] M. Santarsiero, C. Louter, and A. Nussbaumer, "Laminated connections for structural glass applications under tensile loading at different temperatures and strain rates", International Journal of Adhesion and Adhesive. DOI http://dx.doi.org/10.1016/j.ijadhadh.2017.09.002

[25] M. Santarsiero, C. Louter, and A. Nussbaumer, "Laminated connections for structural glass applications under shear loading at different temperatures and strain rates", Construction and Building Materials., vol. 128, 214-237, 2016. http://dx.doi.org/10.1016/j.conbuildmat.2016.10.045

[26] C Bedon, C Louter (2016). Finite-Element analysis of post-tensioned SG-laminated glass beams with mechanically anchored tendons. Glass Structures & Engineering, 1(1): 19-37, doi: 10.1007/s40940-0167

[27] C Bedon, C Louter (2017). Numerical analysis of glass-FRP post-tensioned beams - Review and assessment. Composite Structures, published online, doi: 10.1016/j.compstruct.2017.06.060

[28] CNR-DT 210/2013. Istruzioni per la progettazione, l'esecuzione ed il controllo di costruzioni con elementi strutturali in vetro [Technical Document, in Italian], National Research Council, Rome, Italy (2013)

[29] C Bedon, C Louter (2017). Numerical investigation on structural glass beams with GFRP-embedded rods, including effects of pre-stress. Composite Structures, published online, https://doi.org/10.1016/j.compstruct.2017.10.027

Annex I

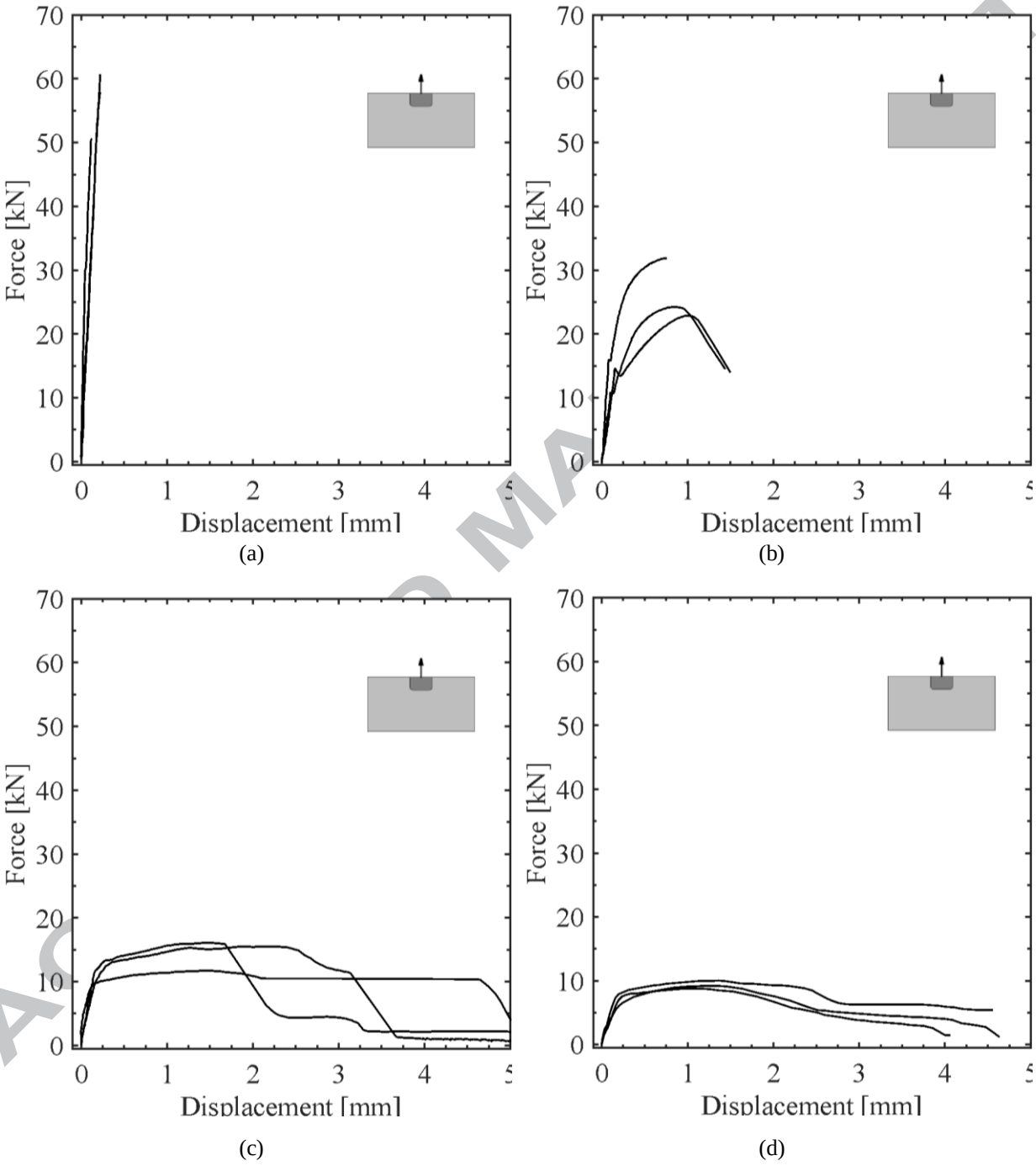

Figure AI-1. Experimental load-displacement curves for thick embedded connections, as obtained for tests at (a) 20°, (b) 40°, (c) 50° and (d) 60°C respectively.

Annex II

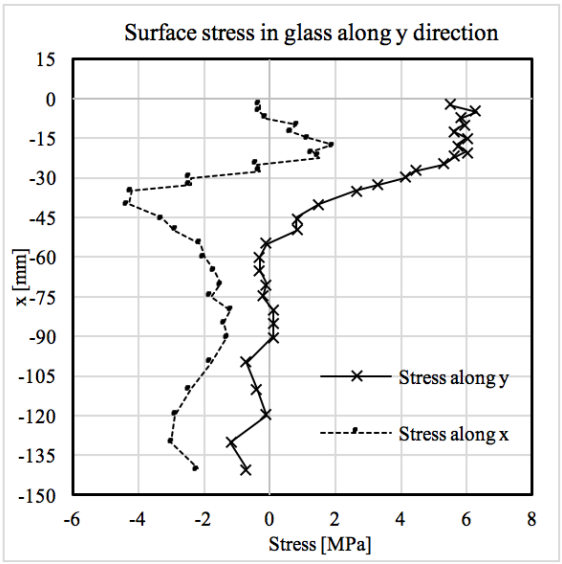

(a)

(b)

Figure AII-2. Residual stress in embedded laminated connection after lamination (a) Stress value along x and y directions (b) Image of specimen with measurements path indicated by dashed line along x-direction, i.e. along symmetry vertical axis. Accuracy of the measurement is given by instrument fabricator as approximately ± 0.5MPa